Smart Antenna Design for 5G and future wireless technologies using Machine Learning Approaches

Final Report

Submitted to the

Telecommunication Regulatory Commission of Sri Lanka

By

R. Valluvan
K. Ahilan
A. Kaneswaran
K. Pirapaharan

Department of Electrical and Electronic Engineering
Faculty of Engineering
University of Jaffna

18-03-2024

Abstract: Smart Antennas are important to provide mobility support for many enhanced 5G and future wireless applications and services such as energy harvesting, virtual reality, Voice over 5G (Vo5G), connected vehicles, Machine-to-Machine Communication (M2M) and Internet of Things (IoT). Smart antenna technology enables us to reduce interference and multipath problems and increase the quality of communication signals. This report presents a number of nonlinear configurations of dipole arrays for forming a single beam in any desired direction. We propose three, four, six and eight elements array structures for the single beamsteering antenna array. Array antenna configurations with multiple axes of symmetry (in the azimuthal plane) models are proposed to decrease the computational repetitions in optimizing respective weight factors for beamsteering. The optimized weight factors are obtained through Least Mean Square (LMS) method. MATLAB™ is used as the software tool to calculate optimized weight factors as well as to determine the resulting radiation patterns. Since antennas are bidirectional elements, beamforming in one direction means that the antenna will also have high receiving gain in that direction. Performance comparison of differently configured models are made in terms of their directivity, sidelobe reduction and computational complexities for beamsteering**.** Smart multiple-input multiple-output (MIMO) antennas with advanced signal processing algorithms are necessary in future wireless networks, such as 6G and beyond, for accurate space division multiplexing and beamforming. Such a MIMO antenna will yield better network coverage and tracking. A smart MIMO antenna configuration with a highly innovative beamforming technique using several nonlinear configurations of dipole arrays. Phase delay factors are optimized at the transmitter to form a single beam and then to steer the beam towards a particular direction. A number of phase shifters are added in order to obtain maximum directional gain. This configuration also significantly increases the power gain of the MIMO antenna at a low cost and with operational simplicity. The paper also demonstrates how the beam width and beamsteering can be effectively controlled. Wolfram Mathematica software was used to generate the three-dimensional radiated beam patterns of the transmitter antenna. There are two approaches to configure the receiver antenna. In the first approach, the received signal magnitude is maximized by aligning the contribution of all elements of the receiver antenna to the same phase. With this approach, the field gain of the proposed system is 25.52 (14.07 dBi). The signal processing gain at the receiver is 64 (18.06 dBi). Therefore, the overall power gain for this proposed new digital/geometrical smart MIMO system is 32.13 dBi. In the second approach, the receiver beam is directed towards the transmitter by optimizing the phase delay coefficients of the receiver. Here, the overall gain of the system is found to be 134.56 (21.28 dBi). Even though the system gain in the second approach is lower, it has the advantage of low interference at the receiver side.

Contents **Page**

1. Introduction. ....……………………………………..1

2. Antenna Array Configurations for a Single Rotatable Beam………………………...…2

3. Digital/Geometrical Hybrid MIMO Beamforming Method.…………………………...…7

4. Beamforming and Beamsteering..10

5. Numerical Evaluations..13

6. Discussions...……………………………………………………………………………25

7. Conclusions……………………………………………………………………………..26

8. References………………………………………………………………………………27

1. Introduction

The emerging 6G and beyond wireless networks will be equipped with accurate user tracking capability using dynamically steered, highly focused radio beams. This will enable enhanced location-based services in addition to space division multiplexing to improve the capacity. These sharply pointed beams will also effectively combat interference in highly crowded heterogeneous environments and efficiently exploit the additional capacity of millimeter wave (mmWave) bands [1,2]. Effective MIMO antennas are required to realize these advanced location- and movement-aware future networks. Such an effective, fast, and low-memory MIMO antenna technique is presented in this paper.

It is well known that MIMO systems use multiple antennas at both the transmitter and receiver to divide and conquer the hostile wireless channel. This can help reduce interference and improve signal quality [4,5]. The MIMO technique exploits multipath propagation, since signals received from multiple paths are intelligently combined at the receiver to reconstruct the original signal [3]. Minimizing interference is achieved by creating nulls in the beam (that is, radiation nulls). In the directions of the beam nulls, the signal is weak or non-existent.

However, the most significant advantage of the MIMO is its beamforming and beam-steering capabilities. Hence, MIMO offers a significant increase in channel capacity without additional bandwidth and it reduces power consumption. The MIMO technology is a key component of many modern wireless communication standards, such as 802.11n and 802.11ac Wi-Fi, and 5G and 6G cellular networks [2,5,6]. With the vast development of MIMO technology, smart MIMO antennas are being intensely researched to improve performance with low hardware and software complexity.

Smart MIMO antennas use advanced signal processing techniques for performance improvement. They have the ability to adapt to changing conditions in the environment, such as the level of interference, in addition to providing user tracking. A smart MIMO antenna can optimize its performance in real time and improve communication speed, capacity, and reliability [7].

Smart antennas are customarily categorized as either switched beam or adaptive array systems based on their operational modes. Switched beam antennas use a finite number of predefined, static, fixed radiation patterns and switch among them as needed. They do not usually use real-time feedback. On the other hand, in an adaptive array antenna system, an infinite number of patterns can be obtained, and these beams can be continuously steered by rapidly adjusting the signal phase angles of each antenna element. For instance, it can dynamically track different types of users, adapt to changing channel conditions, minimize interference, and maximize signal reception by adjusting its parameters in real time [4, 8].

Smart antenna technology can spatially track mobile devices by adapting its radiation pattern to optimize both transmission and reception to/from each user's device [4]. Single beamforming and beamsteering can especially assist in avoiding problematic side lobe radiations.

In order to obtain effective and rotatable beams, signals from multiple elements of a nonlinear antenna array can be appropriately combined. This is achieved by organizing phase delays in the antenna array elements in specified patterns in space [7, 9, 10]. The use of advanced signal processing techniques and artificial intelligence algorithms allows for the optimization of the power and direction of the signal to/from each user, which in turn reduces interference and noise, thereby increasing the communication quality [11].

In this paper, a smart MIMO antenna system is proposed based on the antenna architectures described in [4]. The proposed smart MIMO antenna has the ability to maximize its directional gain by optimizing the phase delay factors of its elements. The validation of this proposed antenna architecture is achieved in a three-dimensional space using Wolfram Mathematica® software. The simulation results show a significant improvement of the directional field and power gains of the proposed system over existing systems. The technique proposed in this paper avoids the usual, costly exercise of adding additional hardware per antenna element (mixers, filters, power amplifiers, etc.) to obtain a high antenna gain. The very significant increase in the power gain is achieved by the smart geometrical arrangement of the MIMO antenna elements and their phase angle optimization. Another advantage of this new MIMO technique is its significantly higher power gain that circumvents the technological limitations and high cost of conventional mmWave electronics to obtain phase shift for every antenna element. Therefore, the technique proposed herein will reduce the cost as well as the complexity of the electronics required.

MIMO beamforming falls under the following categories: analog beamforming, digital beamforming, hybrid (analog/digital) beamforming, and lens-based hybrid beamforming [12]. Analog beamforming is used to improve the signal at the RF level, while digital beamforming is used to improve the signal at the baseband level. The technique presented herein may be the beginning of a new category of MIMO beamforming, which we like to classify as digital/geometrical beamforming. This new digital/geometrical MIMO system can increase the capacity and coverage of wireless links by using a number of beams that can be directed to almost any direction [13]. We assume that this new approach can help overcome some of the following challenges of mmWave 5G and 6G networks: point-to-point predominantly line of sight (LOS) communication, high data rates requiring high network overheads, mobility support, and high user density. With radio networks consuming about 80% of the electric power supplied to mobile networks, the MIMO antenna presented herein is also highly energy efficient, making it an attractive tool in MIMO technology, since MIMO antennas do present an energy consumption problem.

The approach presented in this paper is a novel method of beamforming that utilizes non-numerical optimization techniques to achieve the desired beam. Specifically, the method uses a phase shift technique to manipulate the signal propagation and receiving, allowing for the rapid movement of the beam to new positions without the need for repeated numerical optimizations. This approach offers a significant advantage over traditional methods of beamforming, which rely on probabilistic signal processing techniques that can be time consuming and computationally intensive. By using this innovative technique, the proposed method enables efficient and effective beamforming, making it an important contribution to the field of wireless communication systems.

In section 2, we propose three, four, six and eight elements non-linear arrays for the single beamforming antenna array configurations. Regular polygon array antenna models that has maximum number of symmetrical axes in the azimuthal plane, reduce the computational replication of optimizing the phase delay factors for steering the beam in each direction. On the other hand, these regular polygon models may not provide desired single beam solutions for all angles to be steered. Therefore, we have also studied different array configurations for six and eight element models with multiple symmetrical axes in the azimuthal plane.

In Section 3, we describe the specific construction of the new digital/geometrical MIMO system, both at the transmitter end and the receiver ends, and the geometrical model of the proposed MIMO system. This section also explains how the nonlinearly positioned MIMO antenna in space can be used to form and steer beams by merely shifting the geometric angles of the positions of the elements relative to each other. Since this requires no additional computations, the beams may be steered rapidly. In addition, when the dipole antenna elements are parallel to each other in the MIMO transmitter or receiver, the current elements are parallel to each other, and the vectors of the currents do not come into play. However, in future work, the relative tilt of the transmitter MIMO system with respect to the receiver MIMO system needs to be accounted for.

In Section 4, details of the beamforming and beamsteering approach in the new digital/geometrical MIMO system are given. These equations form the basis of the computer code that is developed to carry out both beamforming and beamsteering. The paper focuses on the generation of a single beam, and not multiple beams, although this technique may be readily extended to multiple beams. In Section 4, the results of a single beam formed using the new digital/geometrical MIMO system are presented. These results ensure pinpoint accuracy, fast steering, low computational burden, and low memory, enabling the system to be able to cater to fast-moving mobile users in low-latency future wireless networks.

2. Antenna Array Configurations for a Single Rotatable Beam

As mentioned previously in [9], the minimum number of dipoles required to steer a single beam in the azimuth angle range (0^0 to 360^0) is three. In the study [9], a three-element equilateral triangular configuration, four-element square configuration and six-element regular hexagonal configuration were proposed for the single beamforming, non-linear array antenna. These configurations are shown in Figure 1. W_1, W_2, W_3, etc… are the complex phase delay factors of the respective antenna elements in the array model.

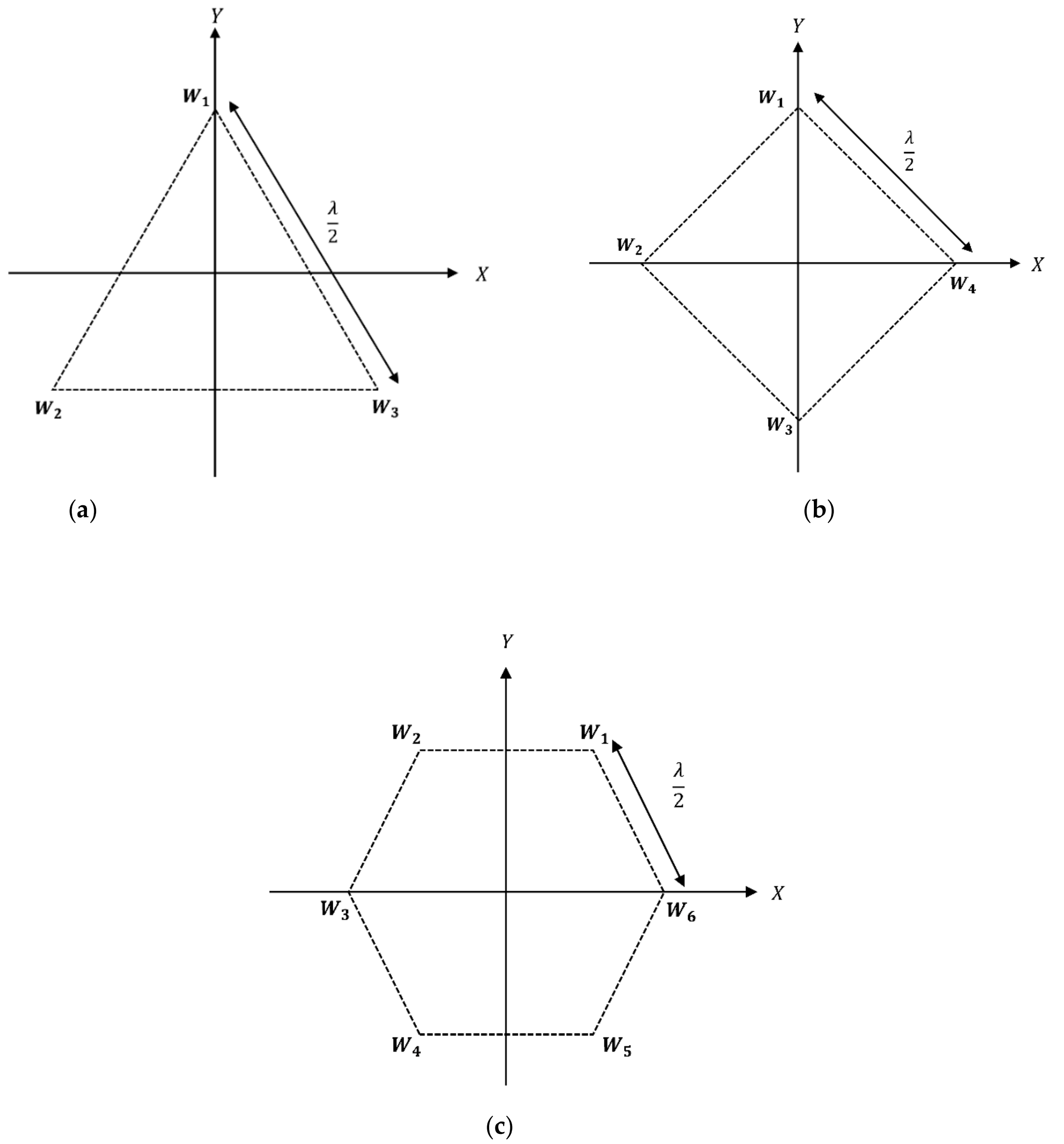

Figure 1. Schematic Diagram of Array Models proposed in [9] (a) Equilateral Triangular Configuration, (b) Square Configuration and (c) Regular Hexagonal Configuration.

When phase delay factors are shifted from end to end vertices, the entire radiation pattern is steered by an angle that the end to end vertices make at the origin. This characteristic will allow us to steer the beam in increments without recalculating the weights when the dipoles are positioned at the vertices of a structure which have multiple axes of symmetry in the azimuthal plane.

In this arrangement, we propose configurations of six-element two-triangular, eight-element regular octagon and two models of two-square antenna array systems to obtain a single, steerable beam for 5G and future applications. Shown in Figure 2 is the schematic diagram of the proposed two-triangular antenna array. The distance between the antenna elements in the larger triangle is $\lambda/2$, and it is $\lambda/4$ for the smaller triangle. W_1, W_2, and W_3 are the complex phase delay factors of the larger triangle and W_4, W_5, and W_6 are the complex phase delay factors of the smaller triangle. Here, to steer the beam to a new direction, we have to simultaneously shift the phase delay factors of both triangles by 120°.

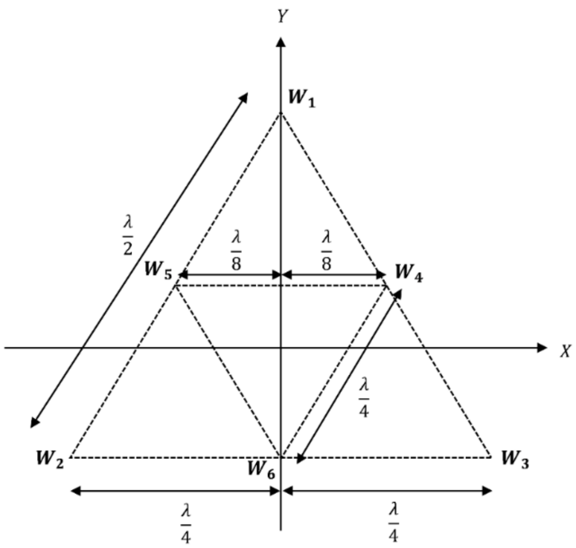

Figure 2. Schematic Diagram of the Proposed Two-Triangular Configuration.

Shown in Figure 3 is the schematic diagram of the proposed regular octagon configuration. The distance between the antenna elements is $\lambda/2$. W1, W2, W3, W4, W5, W6, W7, and W8 are the complex phase delay factors of the vertices of the regular octagon. Here, to steer the beam to a new direction, we have to move the phase delay factors to adjacent vertices by 45°.

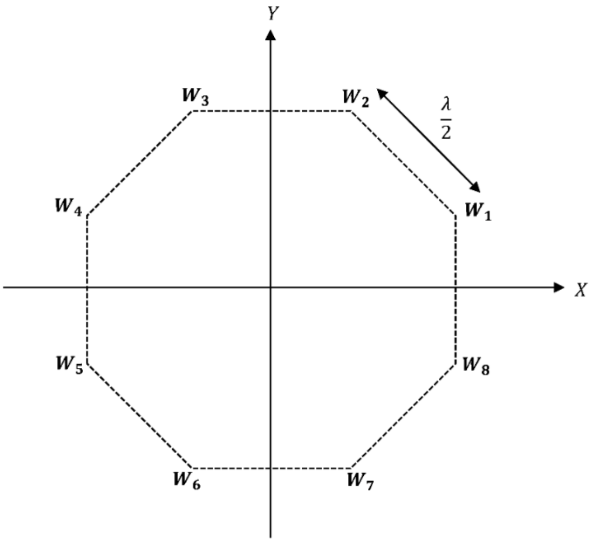

Figure 3. Schematic Diagram of the Proposed Regular Octagon Configuration.

Figures 4 and 5 show the schematic diagrams of the proposed two configurations of two-square antenna arrays. In both configurations, the distance between the antenna elements in the larger square is $\lambda/2$. The distance between the antenna elements in the smaller square is $\sqrt{2}\lambda/4$ in configuration 1 and $\lambda/4$ in configuration 2. W_1, W_2, W_3, and W_4 are the complex phase delay factors of the larger square and W_5, W_6, W_7, and W_8 are the complex phase delay factors of the smaller square. Here, to steer the beam to different direction, we have to shift the phase delay factors of both squares simultaneously to the respective adjacent vertices by 90°.

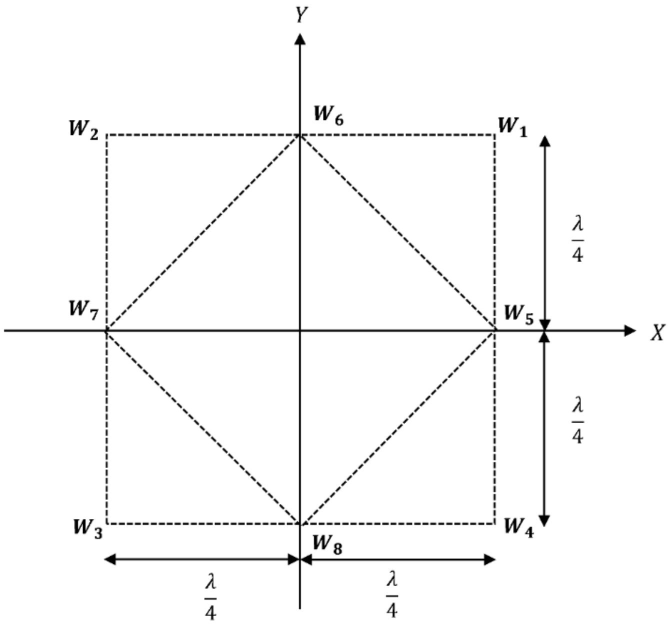

Figure 4. Schematic Diagram of the Proposed Two Square Configuration 1.

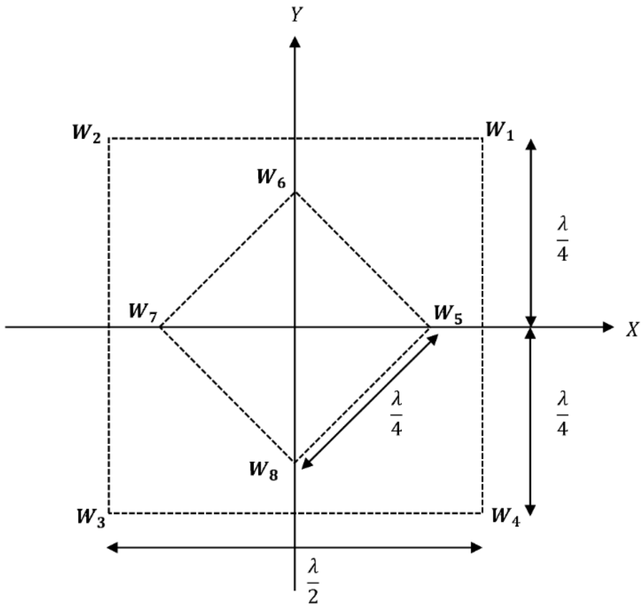

Figure 5. Schematic Diagram of the Proposed Two Square Configuration 2.

When the dipole elements are placed in a regular polygon, as shown in Figure 6, the resulting beam can be advanced by an angle $2\pi/N$, where N is the number of sides of the polygon. Here, the angle between two vertices from the center of the polygon, θ is $2\pi/N$. The mathematics behind this advancement is illustrated in equations (1) to (6).

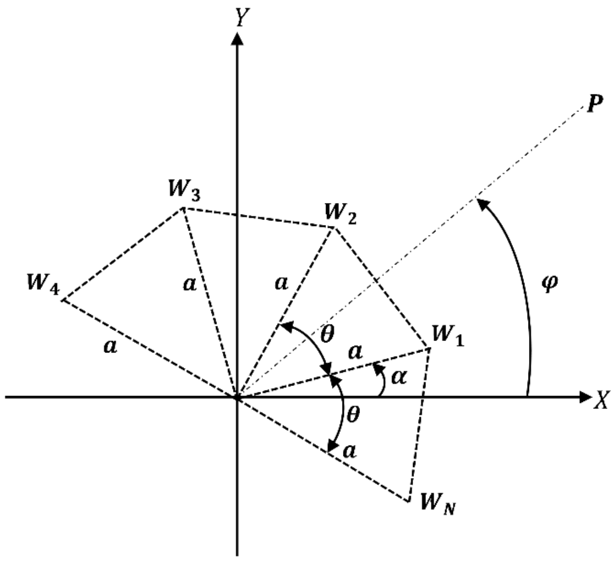

Figure 6. Schematic diagram of dipole placement in a regular polygon.

The electric field at point *P* for the dipoles shown in Figure 6 can be written as:

$$E(\varphi) = W_1 e^{j\beta a\,(\cos\alpha\cos\varphi + \sin\alpha\sin\varphi)} + W_2 e^{j\beta a\,(\cos(\theta+\alpha)\cos\varphi + \sin(\theta+\alpha)\sin\varphi)} + W_3 e^{j\beta a\,(\cos(2\theta+\alpha)\cos\varphi + \sin(2\theta+\alpha)\sin\varphi)} \ldots + W_N e^{j\beta a\,(\cos((N-1)\theta+\alpha)\cos\varphi + \sin((N-1)\theta+\alpha)\sin\varphi)} \quad (1)$$

The equation (1) can be simplified to

$$E(\varphi) = W_1 e^{j\beta\, a\cos(\alpha-\varphi)} + W_2 e^{j\beta\, a\cos(\theta+\alpha-\varphi)} + W_3 e^{j\beta a\cos(2\theta+\alpha-\varphi))} \ldots + W_N e^{j\beta a\cos((N-1)\theta+\alpha-\varphi)} \quad (2)$$

The radiation field at point *P* could be evaluated from equation (2) for arbitrary phase delay factors. For the model shown in Figure 7, we name the element with weight W_1 as the 1st element, that with weight W_2 as the 2nd element and weight W_N as the Nth element, etc. Now we can shift the weights by angle θ so that the 1st element with weight W_N, 2nd element with weight W_1, the 3rd element with W_2 and the Nth element with weight W_{N-1}. For the new weight factors, the radiation field can be obtained using equation (2) and simplified as shown below:

$$\bar{E}(\varphi) = W_N e^{j\beta\, a\cos(\alpha-\varphi)} + W_1 e^{j\beta\, a\cos(\theta+\alpha-\varphi)} + W_2 e^{j\beta a\cos(2\theta+\alpha-\varphi))} \ldots + W_{N-1} e^{j\beta a\cos((N-1)\theta+\alpha-\varphi)} \quad (3)$$

Using the trigonometric identity,

$$\cos(\alpha-\varphi) = \cos(2\pi+\alpha-\varphi) = \cos(N\theta+\alpha-\varphi) \quad (4)$$

We can rewrite equation (3) as:

$$\bar{E}(\varphi) = W_N e^{j\beta\, a\cos(N\theta+\alpha-\varphi)} + W_1 e^{j\beta\, a\cos(\theta+\alpha-\varphi)} + W_2 e^{j\beta a\cos(2\theta+\alpha-\varphi))} \ldots + W_{N-1} e^{j\beta a\cos((N-1)\theta+\alpha-\varphi)} \quad (5)$$

By further rearranging, we can write equation (5) as:

$$\bar{E}(\varphi) = W_1 e^{j\beta\, a\cos(\theta+\alpha-\varphi)} + W_2 e^{j\beta a\cos(\theta+\theta+\alpha-\varphi))} \ldots + W_{N-1} e^{j\beta\, a\cos(\theta+(N-2)\theta+\alpha-\varphi)} + W_N e^{j\beta\, a\cos(\theta+(N-1)\theta+\alpha-\varphi)} = E(\theta+\varphi) \quad (6)$$

Since $\bar{E}(\varphi) = E(\theta+\varphi)$ By shifting the weights to end to end vertices, we may say that the entire radiation pattern can be steered by the same angle. This will allow steering the beam in the steps of the same angle without reevaluating the weights.

3. Digital/Geometrical Hybrid MIMO Beamforming Method

3.1. Proposed Smart MIMO System Architecture

Figure 7 and Figure 8 illustrate the MIMO system architecture, which has multiple antennas at both the transmitter and the receiver. Phase shifters can perform beamsteering and beamforming very quickly with a much higher directional gain. In this MIMO system, the transmitter and the receiver are bidirectional and interchangeable.

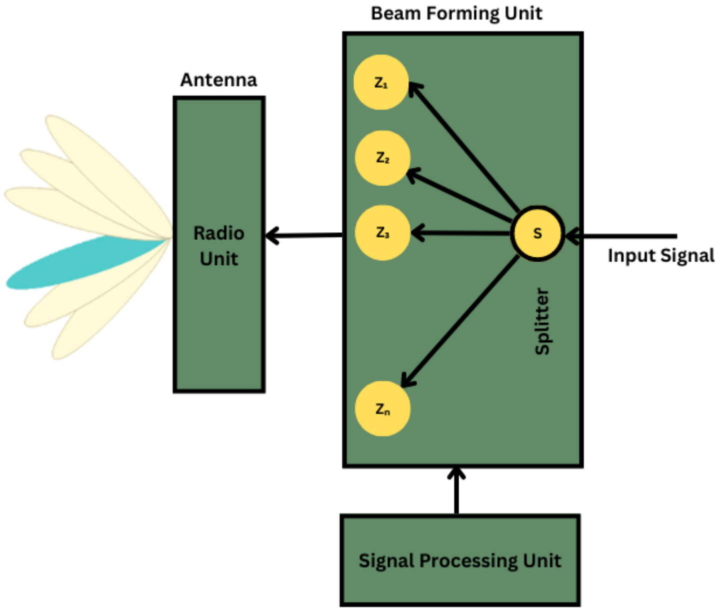

Figure 7. Transmitter antenna of the proposed MIMO system.

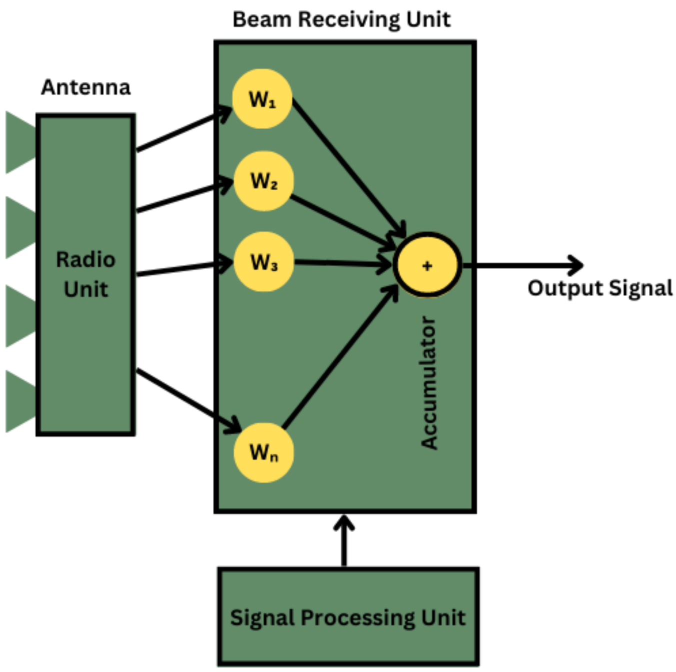

Figure 8. Receiver antenna of the proposed MIMO system.

3.2. Mathematical Modeling of the Smart MIMO System

The proposed new digital/geometrical smart MIMO antenna scheme of this paper can be illustrated using Figure 9 in the XY coordinates system. The transmitter (Tx) has *N* number of multiple antenna elements, with each element positioned in the XY coordinates plane at (x_1,y_1), (x_2,y_2), (x_3,y_3), …, (x_n,y_n). The receiver (Rx) has *M* number of antenna elements, with each element positioned in the UV coordinates plane at (u_1,v_1), (u_2,v_2), (u_3,v_3), …, (u_n,v_n). r is the distance between the reference points of the transmitter antenna and the receiver antenna elements.

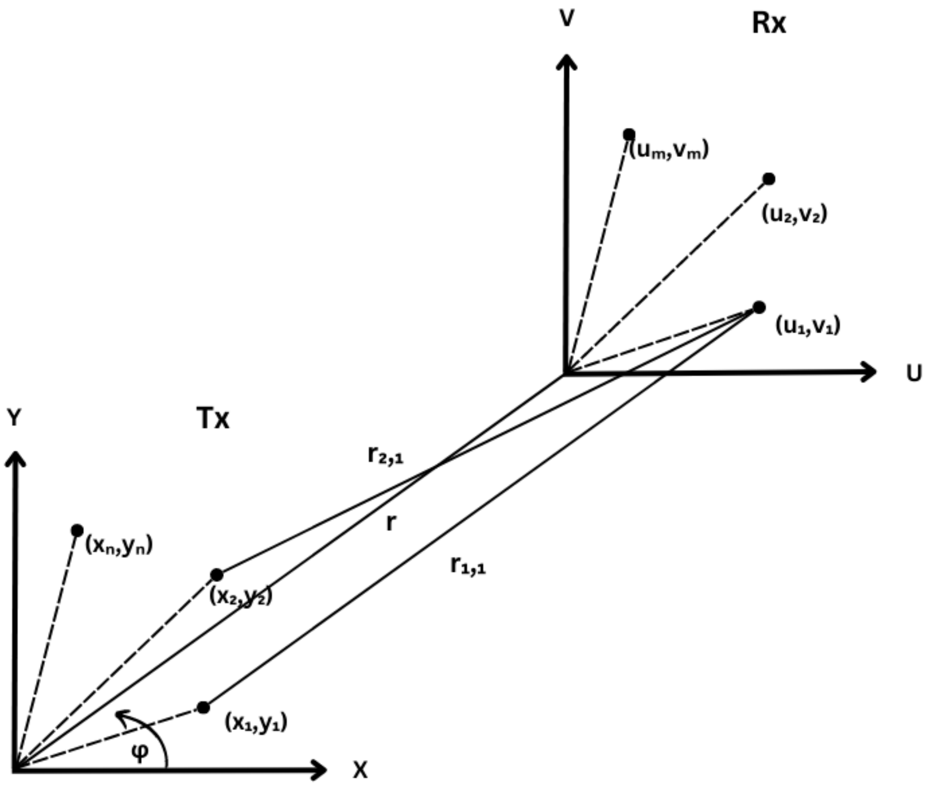

Figure 9. Schematic diagram of the MIMO antenna on XY and UV coordinate planes.

Referring to Figure 9, the distance between the first antenna element of the transmitter and the first antenna element of the receiver can be written as

$$r_{1,1} = r - x_1\cos(\varphi) - y_1\sin(\varphi) + u_1\cos(\varphi) + v_1\sin(\varphi)$$

The distance between the second antenna element of the transmitter and the first antenna element of the receiver can be written as

$$r_{2,1} = r - x_2\cos(\varphi) - y_2\sin(\varphi) + u_1\cos(\varphi) + v_1\sin(\varphi)$$

Similarly, the distance between the n^{th} antenna element of the transmitter and the m^{th} antenna element of the receiver can be written as

$$r_{n,m} = r - x_n\cos(\varphi) - y_n\sin(\varphi) + u_m\cos(\varphi) + v_m\sin(\varphi)$$

With the assumption that all of the transmitter antenna elements have the same length and the same current distribution function along the dipole elements, the vertical plane radiation function $f_{tx}(\theta)$ for all of the transmitter elements are the same. Here, θ is the angle that the observation point makes with the vertical axis of the dipole element. Similarly, with the same assumption, we can also say that the vertical plane radiation function $f_{rx}(\theta)$ of the receiver antenna elements remains same for the receiver elements. Therefore, the entire electric field (E) at the receiver can be written as follows, by incorporating the transmitter and receiver models shown in Figure 7 and Figure 8:

$$E = \Bigg\{ f_{tx}(\theta) f_{rx}(\theta) \left[\frac{e^{-j\beta r_{1,1}}}{r_{1,1}} Z_1 W_1 + \frac{e^{-j\beta r_{2,1}}}{r_{2,1}} Z_2 W_1 + \cdots \frac{e^{-j\beta r_{n,1}}}{r_{n,1}} Z_n W_1 \right] + \left[\frac{e^{-j\beta r_{1,2}}}{r_{1,2}} Z_1 W_2 + \frac{e^{-j\beta r_{2,2}}}{r_{2,2}} Z_2 W_2 + \cdots \frac{e^{-j\beta r_{n,2}}}{r_{n,2}} Z_n W_2 \right] + \cdots + \left[\frac{e^{-j\beta r_{1,m}}}{r_{1,m}} Z_1 W_m + \frac{e^{-j\beta r_{2,m}}}{r_{2,m}} Z_2 W_m + \cdots + \frac{e^{-j\beta r_{n,m}}}{r_{n,m}} Z_n W_m \right] \Bigg\} \quad (7)$$

where β is the phase constant of the radiating wave, W_j are the phase delay factors of the receiving antenna, and Z_i are the phase delay factors of the transmitting antenna. Here, the dipole current I_i is replaced with phase delay factors $Z_i = AI_i$ and A is the constant related to the respective current vectors I_i with the respective phase delay factors Z_i. The vertical plane radiation function of a dipole antenna $f(\theta)$ is given below [26].

$$f(\theta) = \frac{\cos\left(\frac{\beta l}{2}\cos(\theta)\right) - \cos\left(\frac{\beta l}{2}\right)}{\sin(\theta)} \quad (8)$$

where l is the length of the dipole element.

Substituting the expressions for the distances in Equation (7) and rearranging the equation by assuming that all of the distances are equal to r for the amplitude component of the far electrical field, we obtain

$$E = \frac{e^{-j\beta r}}{r} f_{tx}(\theta) \sum_{i=1}^{N} Z_i \, e^{j\beta(x_i cos\varphi + y_i sin\varphi)} \left(f_{rx}(\theta) \sum_{j=1}^{M} W_j \, e^{-j\beta(u_j cos\varphi + v_j sin\varphi)} \right) \quad (9)$$

In order to maximize the directional gain at the receiver, we need to obtain

$$E = \left| \frac{e^{-j\beta r}}{r} \right| \left| f_{tx}(\theta) \sum_{i=1}^{N} Z_i e^{j\beta(x_i cos\varphi + y_i sin\varphi)} \right|_{max} \left| f_{rx}(\theta) \sum_{j=1}^{M} W_j e^{-j\beta(u_j cos\varphi + v_j sin\varphi)} \right|_{max} \quad (10)$$

Expressing the phase delay factor as $W_j = e^{j\beta(u_j cos\varphi + v_j sin\varphi)}$, which is the conjugate value of each receiving antenna element weight, and multiplying each individual term with its conjugate, the maximum directional gain can be achieved.

$$|E|_{max} = \left| \frac{e^{-j\beta r}}{r} \right| \left| f_{tx}(\theta) \sum_{i=1}^{N} Z_i e^{j\beta(x_i cos\varphi + y_i sin\varphi)} \right|_{max} f_{rx}(\theta) M \quad (11)$$

where M is the number of receiving antenna elements.

At the transmitter, the directional beam is to be maximized towards the receiver. In order to obtain $\left(\left|\sum_{i=1}^{N} Z_i e^{j\beta(x_i cos\varphi + y_i sin\varphi)}\right|_{max}\right)$, we enhanced the single beamforming and beamsteering towards receiver direction by optimizing the phase delay coefficients Z_i.

The directivity of an antenna is defined as the ratio of the power radiation intensity in a given direction from the antenna to the power radiation intensity averaged over all directions around the antenna. The directivity D of an antenna in a specified direction is defined from its definition, as below:

$$D = \frac{Power\ Density\ at\ the\ specified\ Direction}{\frac{Total\ Radiated\ Power}{The\ surface\ area\ of\ a\ sphere\ enclosed}}$$

Based on the above definition, we derived Equation (12) for the directivity of the transmitter antenna.

$$D = \frac{2}{\pi} \frac{\left[|f_{tx}(\theta)|^2 \left|E_\varphi\right|^2\right]}{\frac{1}{PQ}\sum_{i=1}^{P}\sum_{j=1}^{Q}|f_{tx}(\theta)|^2 \left|E_\varphi\right|^2 sin\theta} \quad (12)$$

where $E_\varphi = \sum_{i=1}^{N} Z_i e^{j\beta(x_i cos\varphi + y_i sin\varphi)}$. The overall power gain G can be calculated for the system described in Equation (11) as per Equation (13) given below.

$$G = D_{Tx} \times M^2 \times R \quad (13)$$

where D_{tx} is the directivity of the transmitter antenna, M^2 is the signal processing power gain at the receiver antenna, and R is the directivity obtained from the $f_{rx}(\theta)$ function.
The receiving antenna can also perform beamforming and direct the beam towards the transmitter direction. In that case, the overall gain of the system described in Equation (10) can be determined as given in Equation (14).

$$G = D_{Tx} \times D_{Rx} \quad (14)$$

where D_{Rx} is the directivity of receiver antenna. Having beamformed the transmitter and the receiver by steering the transmitter and receiver beams towards each other, the interaction noise received at the receiver is minimized.

4. Beamforming and Beamsteering

Any arbitrary set of dipoles arranged in a uniform linear array produces a symmetrical radiation pattern on both sides of the plane on which the dipoles are placed. However, this arrangement cannot generate a single beam and steer it over the entire space surrounding the antenna. The proposed antenna [4] is a dipole antenna array that can form a single beam and steer the beam in any direction using the optimized phase delay factors. Many research studies show different types of techniques [14–16] used for optimizing the phase shifters. Among them, machine learning and artificial intelligence-based techniques are significant in the optimization process. However, these models require high computational power and memory. This report presents a system that uses a simple mathematical model to optimize the phase delay factors.

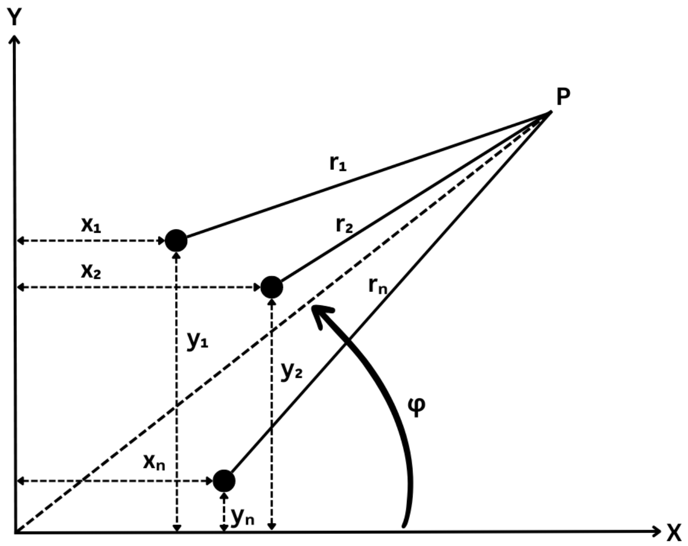

Figure 10. Schematic diagram of dipole placement in XY coordinate plane.

The radiated electric field at a particular point can be written in terms of antenna element current vectors I_1, I_2, I_3, …, I_n for the *N* number of dipoles.

$$E = P_0 I_1 e^{-j\beta r_1} + P_0 I_2 e^{-j\beta r_2} + \cdots + P_0 I_n e^{-j\beta r_n} \tag{15}$$

where $P_0 = A f_{tx}(\theta)$. Substituting for spherical coordinate distances r_1, r_2, and r_n by Cartesian X-Y coordinate distances, Equation (15) can be written as follows, recollecting that $AI_i = Z_i$:

$$E = f_{tx}(\theta) \begin{pmatrix} Z_1 e^{j\beta(x_1 cos\varphi + y_1 sin\varphi)} + Z_2 e^{j\beta(x_2 cos\varphi + y_2 sin\varphi)} + \cdots \\ + Z_n e^{j\beta(x_n cos\varphi + y_n sin\varphi)} \end{pmatrix} \tag{16}$$

where Z_1, Z_2, and Z_n are the complex weights that are proportional to the complex current vectors I_1, I_2, and I_n, respectively. To achieve the objective of forming a resultant single beam, the values of the complex weights Z_1, Z_2, and Z_n need to be optimized such that the resultant radiated field must match a desired single beam function $f(\varphi)$. In order to optimize the phase delay factors to obtain a steerable single beam, a desired single beam function $f(\varphi)$ is selected, as shown in Equation (17).

$$f(\varphi) = Z_1 e^{j\beta(x_1 cos\varphi + y_1 sin\varphi)} + Z_2 e^{j\beta(x_2 cos\varphi + y_2 sin\varphi)} + \cdots + Z_n e^{j\beta(x_n cos\varphi + y_n sin\varphi)} \tag{17}$$

The optimization of complex weights Z_1, Z_2, and Z_n may be achieved either analytically or iteratively [16]. Since the number of dipole elements will be limited to as few as possible, an analytical optimization method is more appropriate.

Complex weights Z_1, Z_2, and Z_n can be optimized by multiplying the equation by its complex conjugates and integrating the φ over the limit from 0 to 2π. Here, the first term is multiplied with the $e^{j\beta(x_1 cos\varphi + y_1 sin\varphi)}$ and integrated with respect to the angle φ over the limits from 0 to 2π. Thus,

$$\int_0^{2\pi} f(\varphi)e^{-j\beta(x_1 cos\varphi + y_1 sin\varphi)}d\varphi = Z_1\int_0^{2\pi} d\varphi + Z_2\int_0^{2\pi} e^{j\beta[(x_2 cos\varphi + y_2 sin\varphi) - (x_1 cos\varphi + y_1 sin\varphi)]}d\varphi$$
$$+ \cdots + Z_n\int_0^{2\pi} e^{j\beta[(x_n cos\varphi + y_n sin\varphi) - (x_1 cos\varphi + y_1 sin\varphi)]}d\varphi \tag{18}$$

249 Similarly, multiplying Equation (17) with the complex conjugates of the second term and integrating
250 over 0 to 2π, we obtain Equation (19),

$$\int_0^{2\pi} f(\varphi)e^{-j\beta(x_2 cos\varphi + y_2 sin\varphi)}d\varphi = Z_1\int_0^{2\pi} e^{j\beta[(x_1 cos\varphi + y_1 sin\varphi) - (x_2 cos\varphi + y_2 sin\varphi)]}d\varphi + Z_2\int_0^{2\pi} d\varphi$$
$$+ \cdots + Z_n\int_0^{2\pi} e^{j\beta[(x_n cos\varphi + y_n sin\varphi) - (x_2 cos\varphi + y_2 sin\varphi)]}d\varphi \tag{19}$$

251 and repeat up to the nth term.

$$\int_0^{2\pi} f(\varphi)e^{-j\beta(x_2 cos\varphi + y_2 sin\varphi)}d\varphi = Z_1\int_0^{2\pi} e^{j\beta[(x_1 cos\varphi + y_1 sin\varphi) - (x_n cos\varphi + y_n sin\varphi)]}d\varphi$$
$$+ Z_2\int_0^{2\pi} e^{j\beta[(x_2 cos\varphi + y_2 sin\varphi) - (x_n cos\varphi + y_n sin\varphi)]}d\varphi + \cdots + Z_n\int_0^{2\pi} d\varphi \tag{20}$$

252 Finally, n number of equations can be obtained where n is equal to the number of dipole elements
253 present in the MIMO antenna. Hence, these equations can be written in the following matrix form:

$$\begin{bmatrix} P_{11} & P_{12} & \cdots & P_{1n} \\ P_{21} & P_{22} & \cdots & P_{2n} \\ \cdots & \cdots & \cdots & \cdots \\ P_{n1} & P_{n2} & \cdots & P_{nn} \end{bmatrix} \begin{bmatrix} Z_1 \\ Z_2 \\ \cdots \\ Z_n \end{bmatrix} = \begin{bmatrix} q_1 \\ q_2 \\ \cdots \\ q_n \end{bmatrix} \tag{21}$$

254 where

$$P_{ij} = \int_0^{2\pi} e^{j\beta[(x_j cos\varphi + y_j sin\varphi) - (x_i cos\varphi + y_i sin\varphi)]}d\varphi \tag{22}$$

255 and

$$q_i = \int_0^{2\pi} f(\varphi)e^{-j\beta(x_i cos\varphi + y_i sin\varphi)}d\varphi \tag{23}$$

256 Thus, the optimized coefficients can be obtained from Equation (21), as given below:

$$\begin{bmatrix} Z_1 \\ Z_2 \\ \cdots \\ Z_n \end{bmatrix} = \begin{bmatrix} P_{11} & P_{12} & \cdots & P_{1n} \\ P_{21} & P_{22} & \cdots & P_{2n} \\ \cdots & \cdots & \cdots & \cdots \\ P_{n1} & P_{n2} & \cdots & P_{nn} \end{bmatrix}^{-1} \begin{bmatrix} q_1 \\ q_2 \\ \cdots \\ q_n \end{bmatrix} \tag{24}$$

where the matrix elements P_{ij} and q_i are numerically calculated.

Once the phase delay coefficients are obtained for a selected angle of beamsteering, the electrical field can be evaluated using the expression obtained in Equation (16).

5. Numerical Evaluations

The optimization of the phase delay factors is carried out as per Equation (24) obtained in this paper. MATLAB® programing language is used to evaluate the phase delay coefficients. Unfortunately, MATLAB® does not have an effective way to display three-dimensional solid shapes. Therefore, Wolfram Mathematica® is used to model the relevant three-dimensional solid beam pattern. Initially, the phase delay coefficients are calculated using the developed software code. Subsequently, these coefficients are used to display the azimuthal plane and three-dimensional solid shape radiation patterns.

5(a): Beam Shifting at 30° steps.

In this section, the results generated by the realistic simulations of the array designs shown in Figures 1c, 2, 3, 4 and 5 are reported, in order to demonstrate the single beam pattern and steered beam pattern achieved by these novel array antenna configurations. In order to obtain the smart antenna phase delay elements, we specify an ideal, desired beams in specific directions, to computationally determine the optimized weights. Subsequently we test the optimized weights to determine the beam shapes in other directions with phase shifting. The optimized phase delay factors are obtained through the LMS method. MATLAB™ is used to first optimize the weights in the LMS method, and then to use these optimized weights on the array antennas to obtain the radiation patterns.

Beam patterns generated by six-element array configurations when using the LMS optimization are shown in Figures 11 and 12. After calculating the weight values for 0^0 and 30^0, we can again steer the beam to 60°, 90°, 120°, 150°, 180°, 210°, 240°, 270°, 300°, and 330° for the regular hexagonal configuration as shown in Figure 7 (b). When considering the regular hexagonal configuration, we have perfect beam match at 0^0 but not at 30^0. Therefore, when the desired angle is at 30°, 90°, 150°, 210°, 270°, and 330°, we get a beam pattern with larger beam width than the desired single beam width.

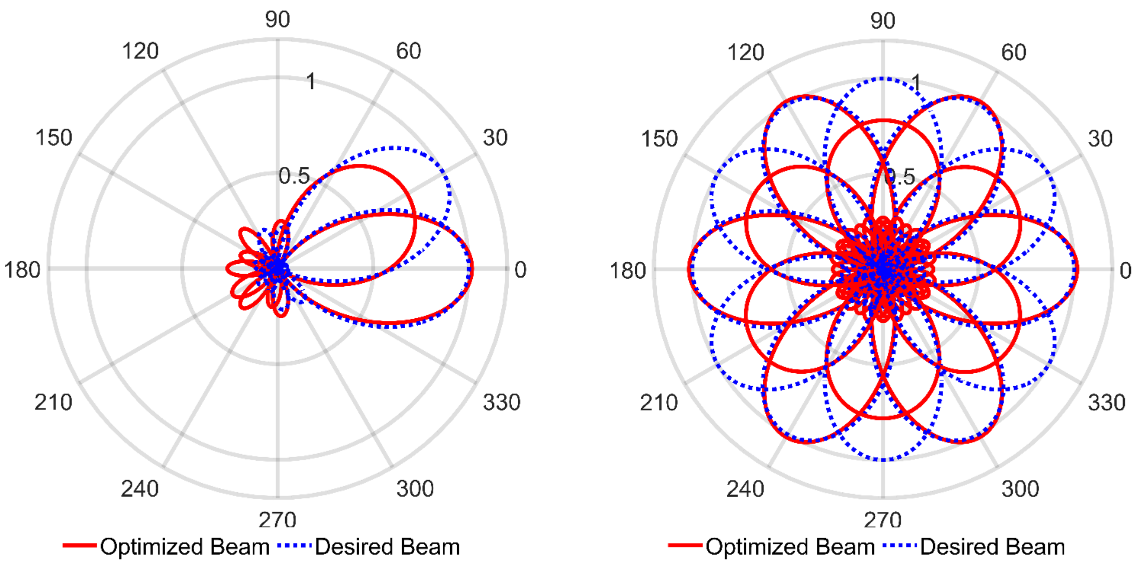

(**a**) (**b**)

Figure 11. Beam Patterns of Regular Hexagonal Configuration (a) Beam to 0^o and 30^o (b) Rotated beams.

In the Two-Triangular Configuration, after calculating the weight values for 0°, 30°, 60°, and 90°, we can again steer the beam to 120°, 150°, 180°, 210°, 240°, 270°, 300°, and 330° as shown in Figure 8 (b). In the two-triangular configuration, we obtained an almost perfect beam match to the desired single beam pattern when the desired angle is 30°, 90° but not at 0°, 60°. Consequently, at 0°, 60°,120°, 180°, 240°, and 300°, we get a beam pattern with larger beam width than the desired single beam pattern. Therefore, we observe that we can steer the beam through 30°, 90°, 150°, 210°, 270°, and 330° with an almost perfect match to the desired beam.

Note that, in the 6-element structure, with reference to one of the dipole positions, five different space vectors exist toward the rest of the dipole positions. Every space vector contributes as different space harmonics (phase shifts) components to direct the beam to the desired direction. The number of space harmonics (five in number) may not be enough to perfectly direct the beam throughout the angle of 0^0 to 360^0. On the other hand, depending on the configuration where the same number of dipoles are placed in different order, we were able to get perfect match at different set of angles. Hence, we can say that by increasing the number of elements and identifying the appropriate dipole positioning configuration, we can have the perfect match for more desired angles. This is tested in the next section.

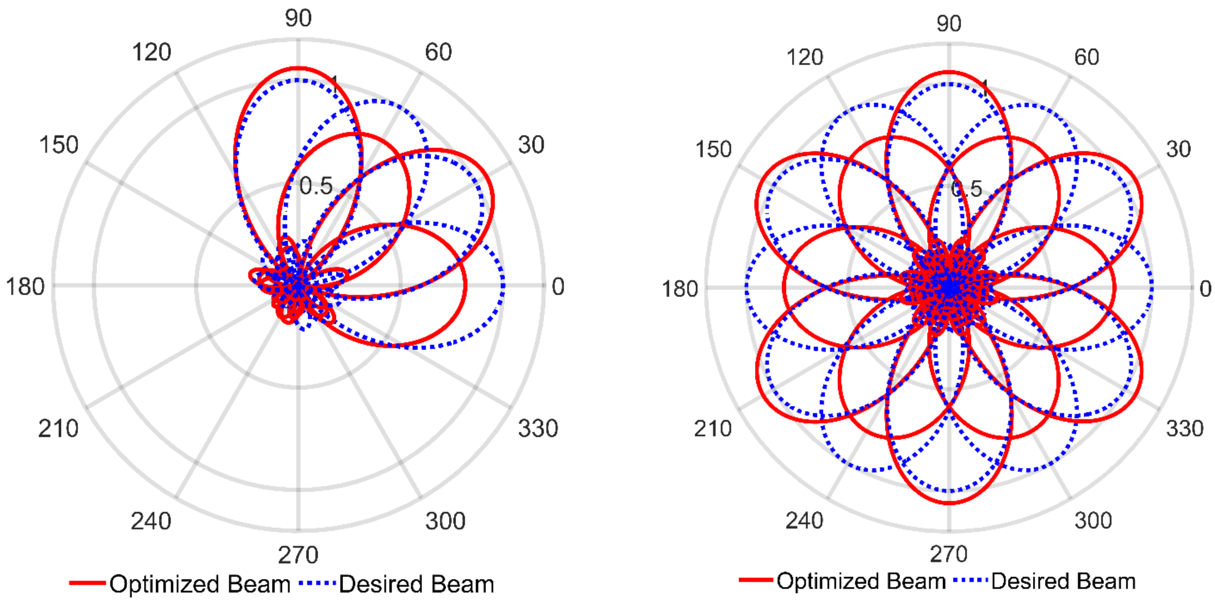

(**a**) (**b**)

Figure 12. Beam Patterns of Two-Triangular Configuration(a) Beam to 0°, 30°, 60°, and 90° (b) Rotated beams.

5(b): Beam Shifting at 15°steps.

It is preferred to steer beam with 15° steps of angles in the regular octagon configuration since there are 8 elements. Having more elements enable us to steer the beam in multiple directions with high accuracy. Having calculated the phase delay factors for 0°, 15°, and 30°, we can again steer the beam to 45°, 60°, 75°, 90°, 105°, 120°, 135°, 150°, 165°, 180°, 195°, 210°, 225°, 240°, 255°, 270°, 285°, 300°, 315°, 330°, and 345° as shown in Figure 13 (b). In the regular octagon configuration, we obtained a narrower beam than desired single beam pattern when the desired angle is 0°, 45°, 90°, 135°, 180°, 225°, 270°, and 315°. When the desired angle is at 15°, 30°, 60°, 75°, 105°, 120°, 150°, 165°, 195°, 210°, 240°, 255°, 285°, 300°, 330°, and 345°, we obtain a beam pattern that could not direct the beam towards the desired direction as shown in Figure 13(b). In addition, for the specific angles, the beam width is larger than the desired beam pattern. Overall, we obtain narrower beams than desired beam at 0°, 45°, 90°, 135°, 180°, 225°, 270°, and 315° while inferior performance at 15°, 30°, 60°, 75°, 105°, 120°, 150°, 165°, 195°, 210°, 240°, 255°, 285°, 300°, 330°, and 345°. The inferior performance is due to the inappropriate positioning of dipole in the stated configuration, so that the beam could not be steered to those particular angles.

Therefore we observe that regular octagonal configuration is not suitable for steering the beam towards all the desired directions though it has the lowest computational requirement to optimize the phase delay factors to do so.

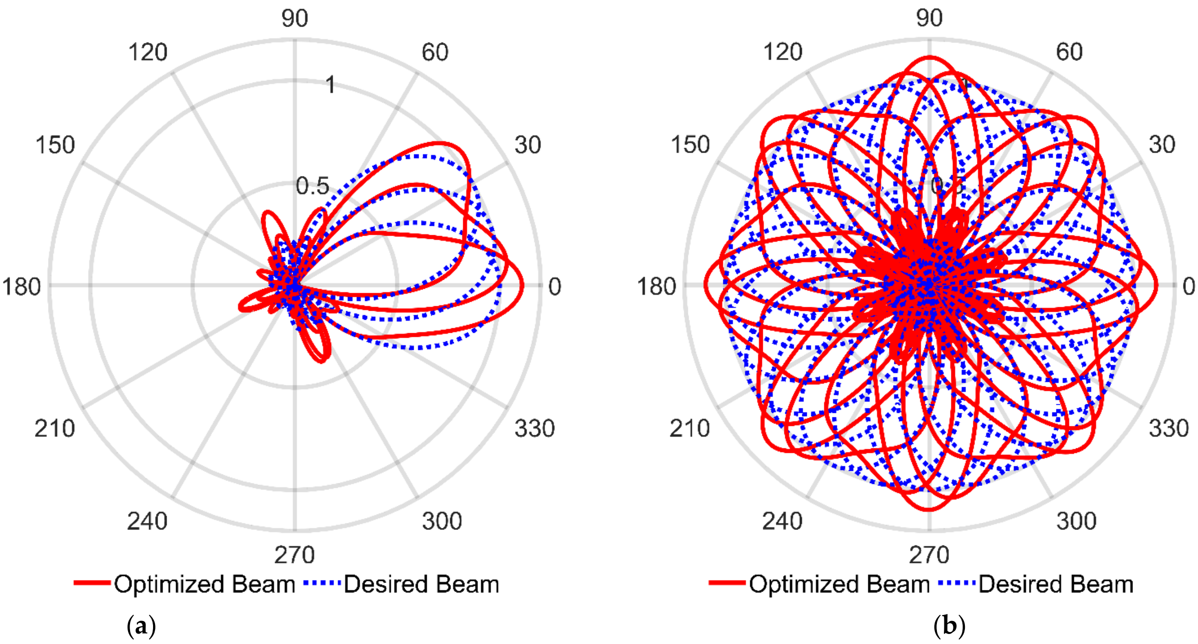

Figure 13. Beam Patterns of Regular Octagon Configuration (a) Beam to 0°, 15°, and 30° (b) Rotated beams.

Since the regular octagonal configuration is unsuccessful for steering the beam in all directions with a good pattern, we consider two special eight-element array configurations which are shown in Figures 14 and 15. Both are named as two-square configurations. Having calculated the weight values for 0°, 15°, 30°, 45°, 60° and 75°, we can again switch the beam to 90°, 105°, 120°, 135°, 150°, 165°, 180°, 195°, 210°, 225°, 240°, 255°, 270°, 285°, 300°, 315°, 330°, and 345° as shown in Figure 14 (b) and Figure 15 (b). In both two-square configurations, we obtained nearly perfect match to the desired beam pattern for all the angles. Therefore, we observe that we can steer the beam in steps of 15^0 from 0^0 to 360^0 with a nearly perfect beam with both two-square configurations.

In the 8-element structure, with reference to one of the dipole positions, seven different space vectors exist toward the rest of the dipole positions. Every space vector contributes different space harmonics (phase shifts) component to direct the beam to the desired direction. The number of space harmonics (7 in number) seems to be enough with appropriate dipole positioning to perfectly direct the beam throughout any desired angle 0^0 to 360^0. Finally, we have shown that while increasing the number of elements and identifying the appropriate dipole positioning configuration, we can have the perfect match for every desired beam angle.

Next we wanted to test if the two-triangular, regular octagon and the both two-square configurations can be used to obtain single beam patterns. We have already shown that regular hexagonal configuration and the proposed two-triangular configuration can be used to obtain nearly perfect match to the desired single beam patterns for some set of angles while the patterns deviate from the desired pattern for another set of angles. Comparing the regular hexagonal and two-triangular configurations, the computational burden is high in the two-triangular configuration for the same set of steering angles. Hence, the regular hexagonal model is superior among these models.

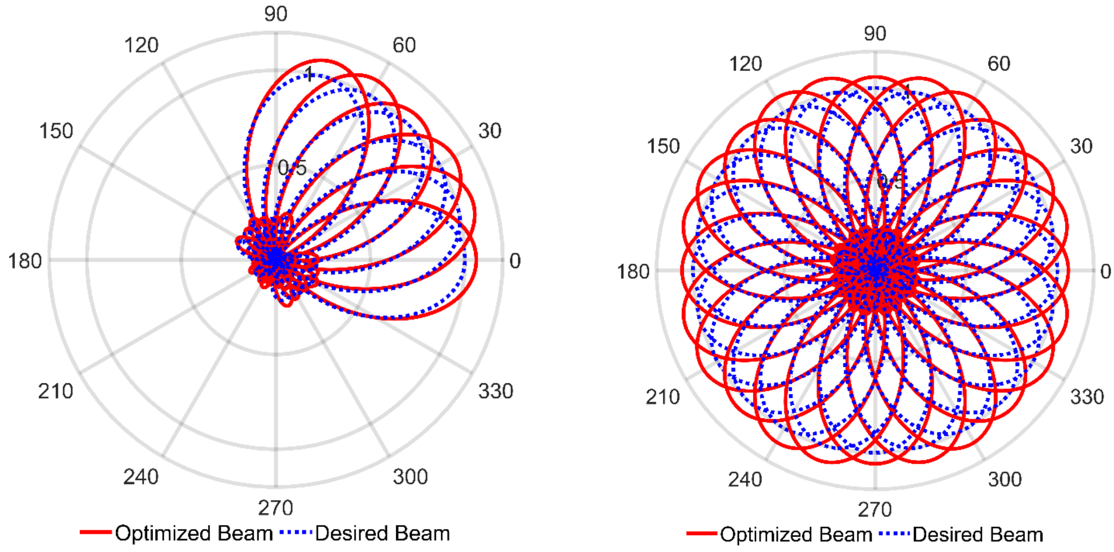

(**a**) (**b**)

Figure 14. Beam Patterns of Two-Square Configuration 1 (a) Beam to 0°, 15°, 30°, 45°, 60°, and 75° (b) Rotated beams.

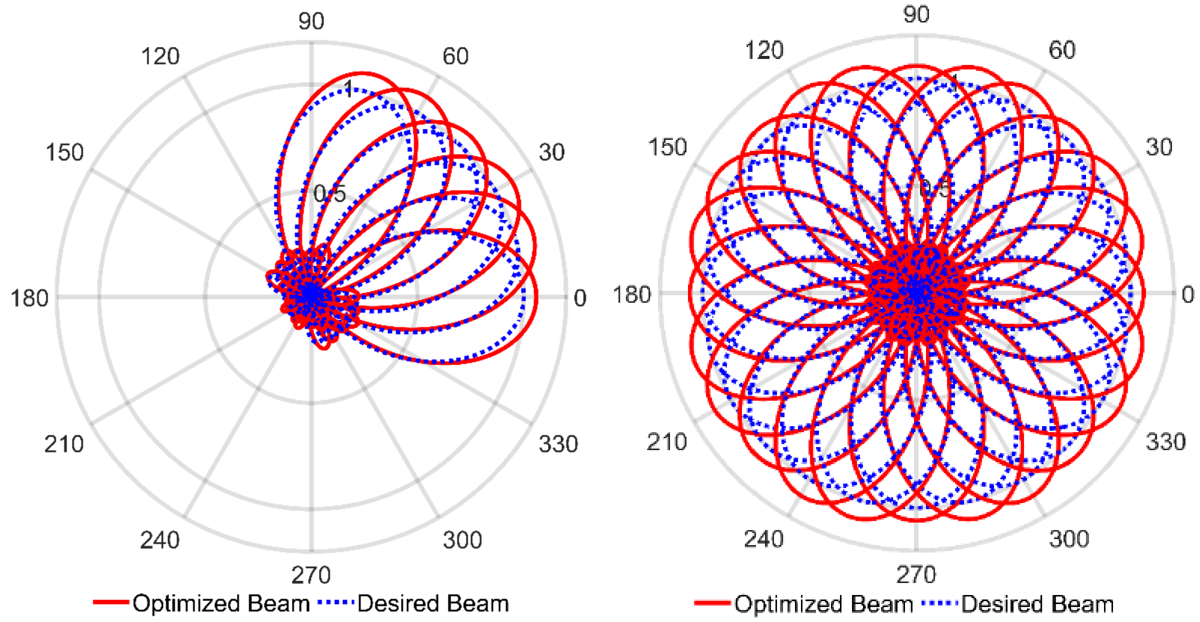

(**a**) (**b**)

Figure 15. Beam Patterns of Two-Square Configuration 2 (a) Beam to 0°, 15°, 30°, 45°, 60°, and 75° (b) Rotated beams.

In the proposed regular octagonal configuration, beam width is narrower with high directivity than the desired single beam in a specific set of directions. However, the beamwidths are wider with poor alignment for another set of angles.

However, in the proposed two-square configurations, nearly perfect beam match to the desired beam pattern is obtained for all possible angles, even though the computational burden is high. Therefore, two-square configurations are superior in performance in comparison to the regular octagonal configuration.

Next, we have optimized the phase delay coefficients to steer beam to 0°, 15°, 30°, 45°, 60° and 75° angles for two square configurations. This proves that the beam can be steered in steps of 15^0 angle from 0^0 to 360 almost perfectly.

5(c): Beamsteering to an Arbitrary Angle.

Finally, for practical applications, the beam has to be steered to any given angle. We have tested this on the two square configuration 1 and two square configuration 2 for angles 10°, 22.5°, 35°, 50°, and 70°. The results are shown in Figure 16 and 17 respectively, where again almost perfect match is achieved. Therefore, we can say that *nearly perfect match for any given angle is possible with both two square configurations studied.*

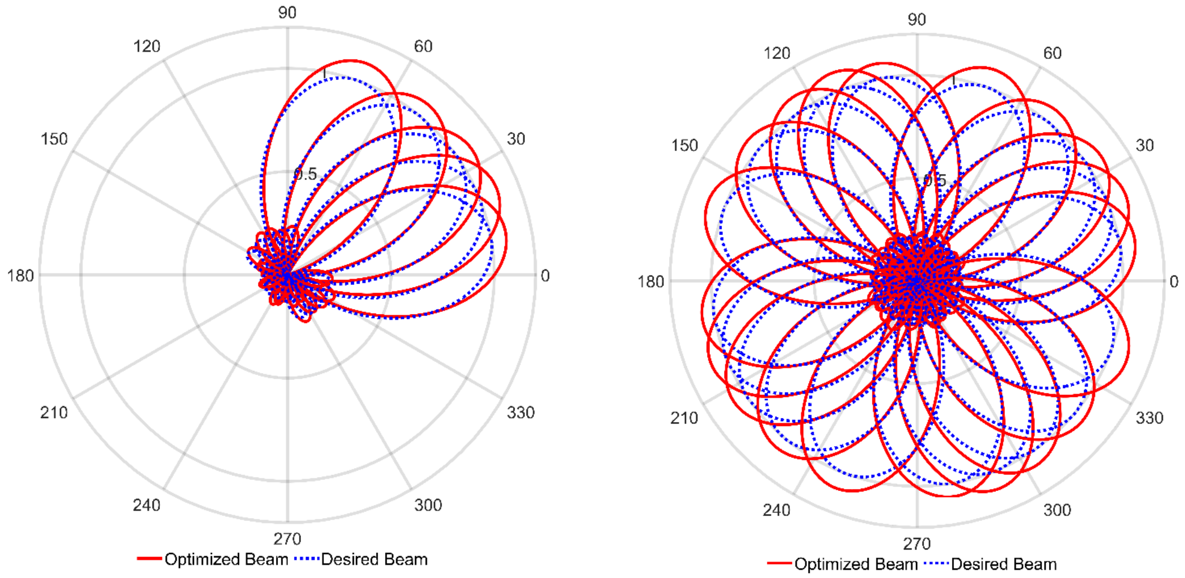

(**a**) (**b**)

Figure 16. Beam Patterns of Two-Square Configuration 1 (a) Beam to random angles 10°, 22.5°, 35°, 50°, and 70° (b) Rotated beams.

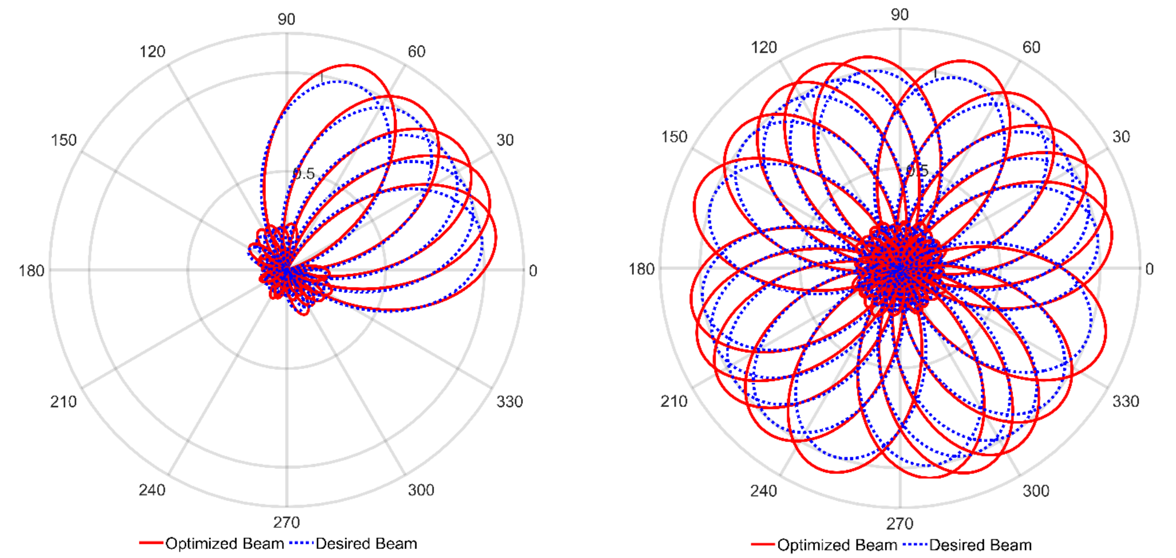

(**a**) (**b**)

Figure 17. Beam Patterns of Two-Square Configuration 2 (a) Beam to random angles 10°, 22.5°, 35°, 50°, and 70° (b) Rotated beams.

5(d): More Observations.

Table 1 and Table 2 summarize the comparison between different nonlinear antenna array configurations to obtain single beam smart antennas. The comparison includes critical factors such as directivity, sidelobe reduction and the accuracy of single beam patterns. These tables demonstrate the effectiveness and advantages of the proposed configurations.

Table 1. Directivity, Sidelobe Reduction and Single Beam Patterns for the Array Models proposed in [9].

Configurations	Optimized Angle	Maximum Directivity	Sidelobe Reduction	Single Beam Patterns
Equilateral Triangular	0°	2.88 at -0.09°	0.38 with the sidelobe located at 138.56°	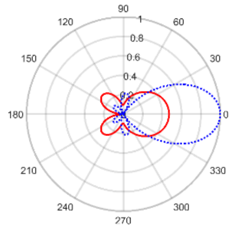
	30°	3.09 at 29.91°	0.73 with the sidelobe located at -150.00°	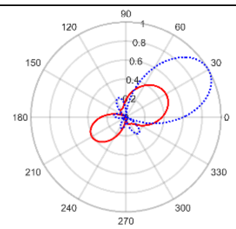
	60°	2.89 at 59.91°	0.41 with the sidelobe located at -76.46°	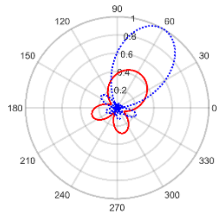
	90°	3.10 at 89.91°	0.70 with the sidelobe located at -90.18°	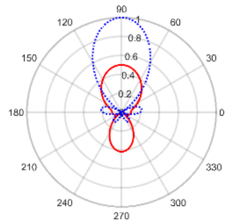
Square	0°	5.09 at -0.09°	0.31 with the sidelobe located at 180.00°	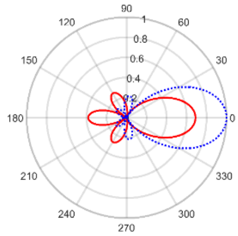

	30°	3.95 at 12.15°	0.56 with the sidelobe located at -128.2276°	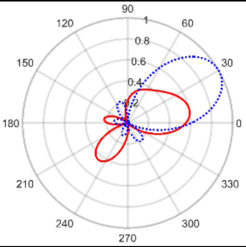
	60°	3.95 at 77.67°	0.56 with the sidelobe located at -141.38°	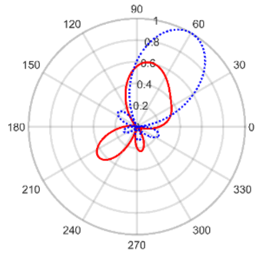
Regular Hexagonal	0°	6.42 at -0.09°	0.08 with the sidelobe located at -133.02°	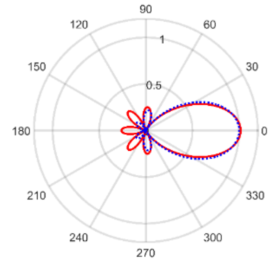
	30°	5.06 at 29.91°	0.12 with the sidelobe located at -150.00°	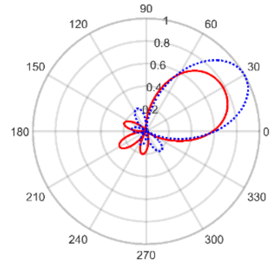

Table 2. Directivity, Sidelobe Reduction and Single Beam Patterns for the newly proposed Array Models.

Configurations	Optimized Angle	Maximum Directivity	Sidelobe Reduction	Single Beam Patterns
Two-Triangular	0°	5.23 at -0.09°	0.05 with the sidelobe located at -107.81°	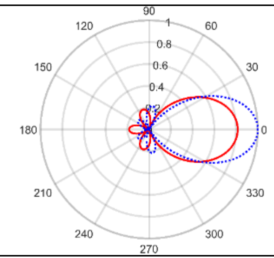
	30°	6.75 at 29.91°	0.05 with the sidelobe located at 106.69°	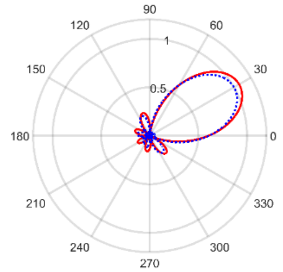

	60°	5.23 at 59.91°	0.06 with the sidelobe located at 168.77°	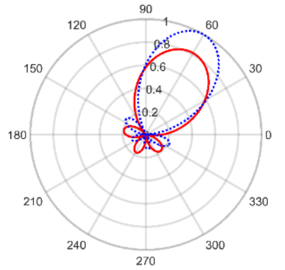
	90°	6.75 at 89.91°	0.05 with the sidelobe located at 13.13°	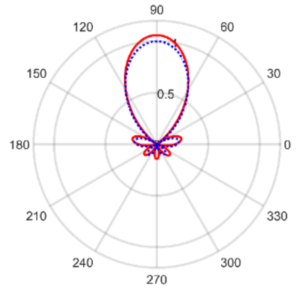
Regular Octagon	0°	7.78 at -0.09°	0.13 with the sidelobe located at 70.38°	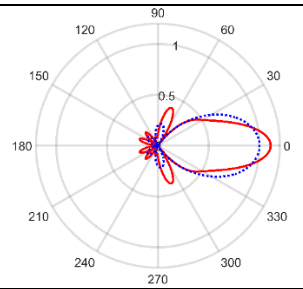
	15°	6.84 at 6.89°	0.14 with the sidelobe located at -66.45°	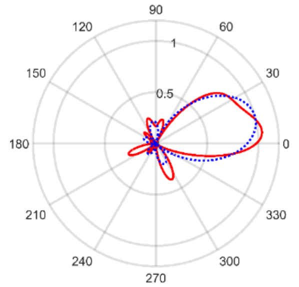
	30°	6.85 at 38.50°	0.14 with the sidelobe located at 111.27°	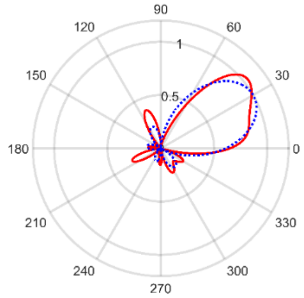

Two Square 1	0°	6.94 at -0.09°	0.06 with the sidelobe located at -75.1487°	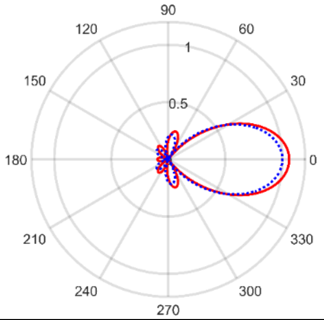
	15°	7.07 at 15.85°	0.05 with the sidelobe located at -62.44°	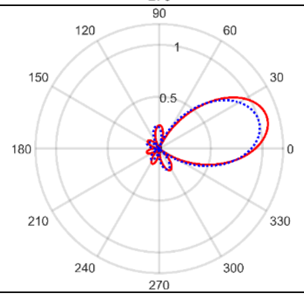
	30°	7.10 at 29.84°	0.04 with the sidelobe located at 107.26°	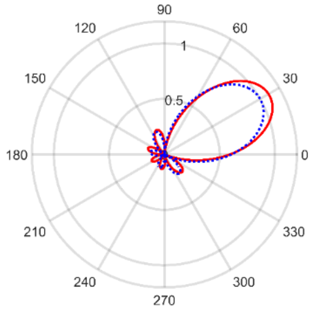
	45°	6.92 at 44.91°	0.06 with the sidelobe located at -30.72°	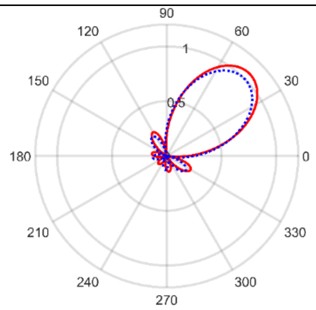
	60°	7.08 at 60.48°	0.05 with the sidelobe located at -17.44°	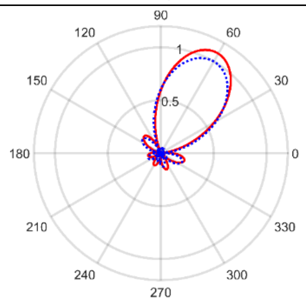

75°	7.08 at 74.76°	0.05 with the sidelobe located at 152.26°	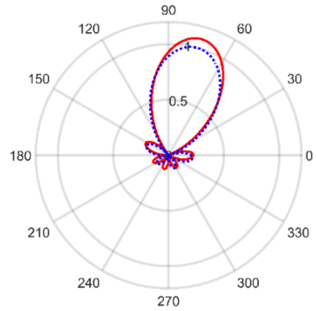

5.2. Beamforming to a Desired Direction

The proposed eight-element dipole antenna configuration from our previous single beam work [4], shown in Figure 18, is used as the transmitter and is optimized to form a beam in arbitrarily selected directions. This antenna can steer the beam to any direction (from 0° to 360°). These outcomes are already validated in our previous work [4] and will not be repeated herein considering space and similarity concerns. However, the radiation patterns are tested to steer the beam towards random angles 0°, 5°, 15°, 27°, 42°, 55°, 73°, 88°, 135°, 152°, 177°, 213°, 245°, 260°, 305°, and 340° by optimizing the phase delay coefficients, as shown in Figure 19.

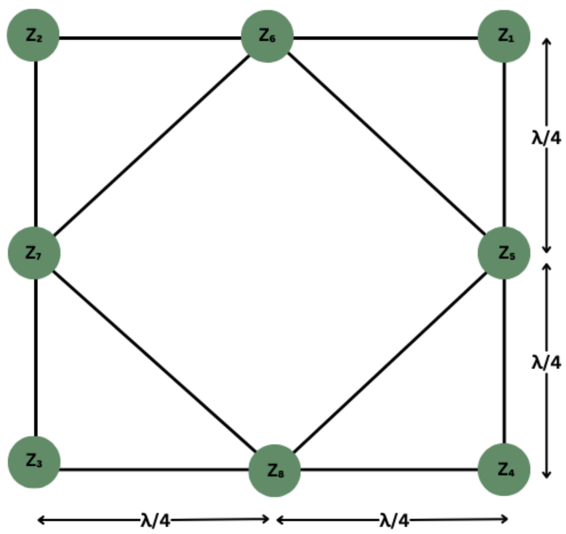

Figure 18. Proposed eight-element dipole antenna.

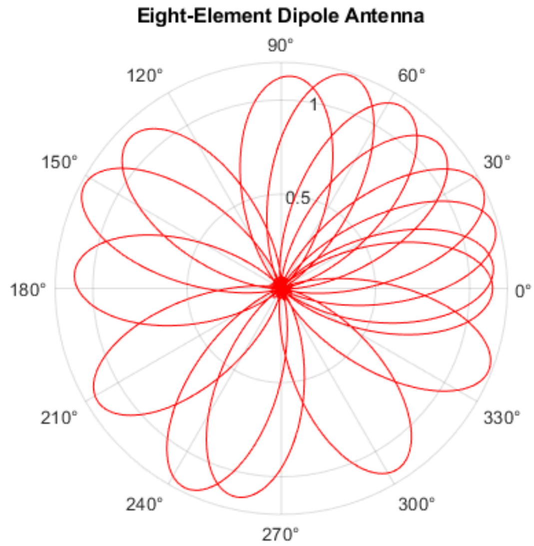

Figure 19. Radiation pattern for arbitrarily steering beams.

We were able to steer a single beam to almost any direction while retaining its shape. The directivity was varied with an accuracy of 0.1^0. Thus, the performance of steerable single beamforming is well proven with high accuracy.

The beam presented in Figures 20–22 was created to study the three-dimensional radiation pattern. This was carried out considering the dipole elements as half-wave dipoles and a randomly selected angle of 30^0. The 3D space views of the obtained beam are presented in Figures 20–23 with the different positions.

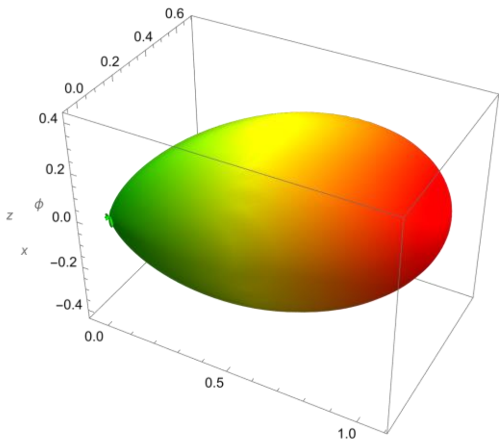

Figure 20. Three-dimensional view of the single beam formed at 30^0 when the transmitter antenna elements are half-wave dipoles.

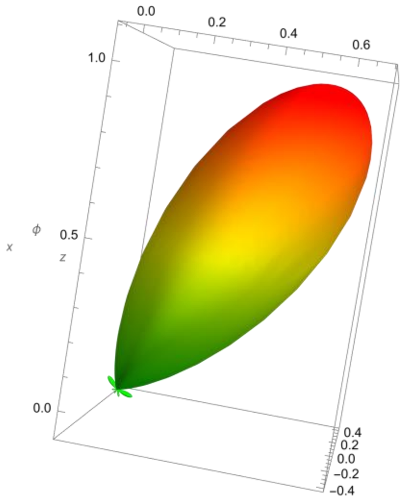

Figure 21. Azimuth view of the formed narrow beam.

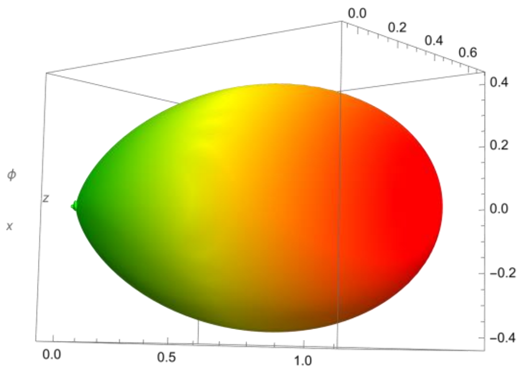

Figure 22. Vertical view of the formed narrow beam.

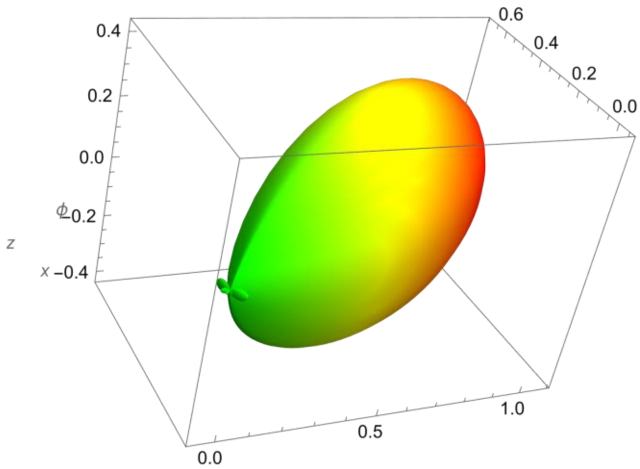

Figure 23. The same beam is shown at an angle for a better view of the side lobes. The side lobes have negligible energy.

Seven different space vectors occur in an eight-element antenna structure. The beam is guided in the desired direction by the contributions of phase shifters from each space vector. Eight phase delay shifters, combined with proper dipole placement positions, are sufficient to precisely guide the beam toward any desired angle between 0° and 360°. The shape of the beam is very narrow and highly focused. Moreover, the energy wastage is negligible due to the negligible side lobes, which illustrates that this antenna is highly energy efficient.

5.3. Performance of Proposed Smart MIMO System

Compared to an isotropic antenna, the directivity of the new digital/geometrical MIMO is very high. This means that it can precisely transmit or receive signals in a specific direction. The directivity of an antenna is expressed as a ratio of the power transmitted or received in a particular direction to the average power radiated or received by an isotropic antenna and is usually measured in decibels (dB). According to the numerical calculation, the directivity of this transmitted beam of the new digital/geometrical MIMO for the example presented above is 11.6 (10.65 dBi), while the obtained side lobe reduction is 0.05. When we use a similar antenna as the receiver end of this system, the eight-element dipoles proved to be a highly directive receiving side. On the receiving side, the directivity of the vertical plane of half-wave dipole antenna affects the overall antenna gain. According to the calculations performed, this value is 2.2 (3.42 dBi) for the proposed MIMO receiver system. Hence, the overall antenna gain for this proposed system is 25.52 (14.07 dBi). Moreover, the signal processing gain at the receiver antenna contributes to the overall power gain of the system. The signal processing gain at the receiver is 64 (18.06 dBi). Therefore, the overall power gain of the proposed new digital/geometrical smart MIMO system, calculated using Equation (7), is 1633.28 (32.13 dBi).

Using Equation (8), we calculated the overall power gain of the MIMO system when both the receiving and transmitting antennas were pointing at each other. This was 134.56 (21.28 dBi).

6. Discussion

From the Tables we observe the following. In the two triangular configuration, better directivity and improved sidelobe reduction are observed than previous results in the proposed configurations at certain angles. However, in some instances, a somewhat larger beam-width is obtained.

Among the previously studied and newly proposed configurations, the regular octagonal configuration gives a beam with the highest directivity for a set of specified desired angles, but with poor sidelobe reduction. For the remaining set of angles, the beam is not formed at the desired angle for maximum radiation.

Both Two Square Configurations provide almost identical beam patterns of the desired beam, directivity and sidelobe reduction. Among the previously proposed and newly proposed configurations, only the two square configurations provide high directivity and improved sidelobe reduction for all angles throughout the 360° space. However, the largest directivity in regular octagonal configuration for a set of angles is greater than that of two square configurations.

In the regular hexagonal and two triangular configurations the computational burden is high in the two-triangular configuration for the same set of steering angles.

In regular octagon and two square configurations, for the same set of steering angles, the computational burden is high in two square configurations. However, almost identical directivity and beamwidth are achieved throughout all the specified angles.

All newly proposed configurations provide higher directivity and improved sidelobe reduction compared to the previously proposed configurations. Furthermore, among the proposed models, the two square configurations provide high directivity and improved sidelobe reduction for all the scanned angles.

Finally we note that the physical realization of these antenna configurations might bring new challenges. Furthermore, the high speed controllable phase delay elements may not be freely available in the market.

MIMO technology has become a key component in modern wireless communication systems, enabling higher data rates, improving reliability, and providing better coverage in challenging environments. This developed antenna system is a novel digital/geometrical MIMO dipole antenna architecture that has high-speed beamsteering capability, which allows the beam to be steered in any direction (0°–360°) with high directionality and low complexity due to the optimization of the phase delay factors.

According to Figures 7–9, the radiated beam is very narrow in all of the three-dimensional planes, proving a high directionality, low interference from/to other sources, and high energy efficiency in a desired direction. Due to these advantages, this new digital/geometrical MIMO system can significantly benefit future wireless communication using 6G and beyond [4].

Furthermore, the directivity of the transmitter is approximately 11.6 (10.65 dBi). Compared with other types of MIMO antenna systems, this directivity value is higher. For instance, in patched-type [17–21] antenna systems, the directivity is between 3 dBi and 10 dBi. Moreover, the patched-type antennas work at a limited frequency band. According to the study and findings of [22], the beam directivity can be increased to 15 dBi using structurally larger and heavier horn-type antennas. However, this beam cannot be steered easily. Furthermore, it requires a considerable amount of energy to form a beam. As we can observe from the radiation patterns of the antenna in [22], much energy is wasted on the intermediate side lobes. Another study on a spiral-dipole antenna elaborated that the power gain of the antenna transmitter is between 0 dBi and 3 dBi. Another MIMO dipole antenna shown in [23] reached the maximum power gain of 4.7–4.9 dBi. A microstrip antenna using metamaterial yielded a maximum power gain value of 15 dBi in [24]. However, the radiated beam is not steerable in all directions, and the energy wastage is high. By comparing the antennas mentioned above, this proposed smart new digital/geometrical MIMO system has several advantages and is a competitive antenna design for future wireless communication systems.

At the receiver side, there are eight dipole elements that are connected to the phase delay factors. Hence, the signal processing gain of the receiver antenna is 64 (18.06 dBi). This gain value contributes to the increase in the overall power gain of the new digital/geometrical MIMO system. Due to the directivity of the vertical plane for a half-wave dipole antenna at a specified angle, the overall power gain value at the receiver-side antenna is 64 * 2.2 = 140.8 (21.48 dBi). Therefore, this proposed system has a very high directional power gain at its receiver end. This will increase the quality of the signals [25] and provide the ability to detect very weak signals from long distances.

The overall power gain of the entire smart MIMO system is 1633.28 (32.13 dBi), which is a very high value when compared with the other types of MIMO systems. However, when we calculated the overall directivity by forming the beams to a specified direction at the transmitter and at the receiver, the overall power gain value only reached 134.56 (21.28 dBi). There is a significant difference between these two values because, when we used the first approach, more noise was generated at the receiving side due to multiple receiving signals. Hence, the SNR of that system was low. However, when the beams were formed to specified directions at the transmitter and receiver, the effect of the noise was very low, leading to a higher SNR value.

One of the advantages of this system is that the transmitter can work as a receiver, and the receiver can work as a transmitter. Even though the directional power gains change with the transmitter or receiver, the overall power gain of the entire system remains the same and will only be changed by inadvertent environmental factors, such as rain or buildings.

7. Conclusions

This paper presents multiple new antenna structures that will perform single beamforming in multiple directions on the move. Namely, two-triangular, regular octagonal and two different two-square single beamsteering non-linear antenna array configurations are proposed for 5G and future 6G energy harvesting applications.

Using the proposed two-square configurations, we can direct the single beam to different angles from 0 to 360°. Furthermore, we have used the array antenna configurations with the multiple axes of symmetry in the azimuthal plane to avoid recalculating the weights when rotating the beams from 0° to 360°. This characteristic enables multiple directional steering of antenna beams for two-square configurations while computing the phase delay factors for only one fourth of the required rotational angles.

Our studies show that by appropriately increasing the number of dipole elements with appropriate positioning them we can achieve smart array antennas that will receive or transmit energy with high directivity and narrow beamwidth from/to any direction. Even though the regular polygon structures have the maximum number of symmetrical axes, regular polygon configurations may not be the best solution to positioning the dipoles to steer the beam throughout 360^0 space. Even though, we have identified suitable configurations with 8 elements, further study on optimal positioning of dipoles, as well as extending this work to non-dipole antenna arrays is a challenging area.

For the next-generation wireless networks, massive MIMO is the essential enabling technology, combining the antenna arrays at the transmitter and the receiver to offer exceptional spectral and energy efficiency. This paper elaborates on the overall performance of the proposed smart MIMO antenna system, namely, the new digital/geometrical MIMO. According to the mathematical formulation of the signal processor, software code implementation, and calculations, the overall gain of the proposed system is 25.52 (14.07 dBi). The signal processing gain at the receiver is 64 (18.06 dBi). Therefore, the overall power gain for this proposed new digital/geometrical smart MIMO system is 1633.28 (32.13 dBi). When we calculate the overall directivity by forming the beams towards a selected direction at the transmitter and the receiver, the overall power gain value increased to 134.56 (21.28 dBi).

The proposed system has several advantages that make it suitable for use in M2M and IoT applications. It can radiate very narrow beams with low energy consumption, and it can form and steer beams in any desired direction. The phase delay shifters can optimize the beamforming to reduce side lobes and improve the overall directivity.

The paper suggests future developments of the work, such as adjusting the transmitter weights to further increase the power gain of the transmitter, improving the performance of the receiver, and eliminating spatially distributed noise by beamforming at the receiver. The implementation of the physical antenna structure is planned to evaluate and fine tune its hardware performance, making it readily available for use in 5G and 6G wireless systems and beyond.

Overall, the proposed digital/geometrical MIMO system shows promising results for achieving high spectral and energy efficiency in wireless networks, and its potential applications in M2M and IoT make it an interesting technology to watch in the future.

References

1. Chataut, R.; Akl, R. Massive MIMO Systems for 5G and beyond Networks—Overview, Recent Trends, Challenges, and Future Research Direction. *Sensors* **2020**, *20*, 2753. https://doi.org/10.3390/s20102753.
2. Sharma, P.; Tiwari, R.N.; Singh, P.; Kumar, P.; Kanaujia, B.K. MIMO Antennas: Design Approaches, Techniques and Applications. *Sensors* **2022**, *22*, 7813. https://doi.org/10.3390/s22207813.
3. Patil, A.; Bhadade, R.S. A Literature Survey on MIMO Antenna. In Proceedings of the 2nd International Conference on IoT based Control Networks & Intelligent Systems (ICICNIS), Kottayam, India, 28-29 June 2021: pp.1-9. https://doi.org/10.2139/ssrn.3884043.
4. Pirapaharan, K.; Ajithkumar, N.; Sarujan, K.; Fernando, X.; Hoole, P.R.P. Smart, Fast, and Low Memory Beam-Steering Antenna Configurations for 5G and Future Wireless Systems. *Electronics* **2022**, *11*, 2658. https://doi.org/10.3390/electronics11172658.
5. Mubeen, S.; Prasad, A.M.; Rani, A.J. Smart Antennas Implementation for MIMO. *J. Inf. Eng. Appl.* **2012**, *2*, 9–16.
6. Yerrapragada, A.K.; Kelley, B. On the Application of K-User MIMO for 6G Enhanced Mobile Broadband. *Sensors* **2020**, *20*, 6252. https://doi.org/10.3390/s20216252.
7. Supriya, R.; Kumar, D.S. Adaptive Algorithms in Smart Antenna Beamformation for Wireless Communication. In Proceedings of the 2016 International Conference on Communication and Signal Processing (ICCSP), Melmaruvathur, Tamilnadu, India, 6–8 April 2016; pp. 1850–1853.
8. Inzillo, V.; De Rango, F.; Zampogna, L.; A. Quintana, A. Smart Antenna Systems Model Simulation Design for 5G Wireless Network Systems. In *Array Pattern Optimization*; Mohammed, J.R., Sayidmarie, K.H., Eds.; IntechOpen: London, UK, 2019; ISBN 978-1-78985-741-2.
9. Pirapaharan, K.; Kunsei, H.; Senthilkumar, K. S.; Hoole, P. R. P.; Hoole, S. R. H. A Single Beam Smart Antenna for Wireless Communication in a Highly Reflective and Narrow Environment. In *2016 International Symposium on Fundamentals of Electrical Engineering (ISFEE)*; 2016; pp 1–5. https://doi.org/10.1109/ISFEE.2016.7803214.
10. Ardi, E.M.; Shubair, R.M.; Mualla, M.E. Adaptive Beamforming Arrays for Smart Antenna Systems: A Comprehensive Performance Study. In Proceedings of the IEEE Antennas and Propagation Society Symposium, Monterey, CA, USA, 20–25 June 2004; Vol.3, pp. 2651–2654
11. Singh, A.; Kumar, A.; Ranjan, A.; Kumar, A.; Kumar, A. Beam Steering in Antenna. In Proceedings of the 2017 International Conference on Innovations in Information, Embedded and Communication Systems (ICIIECS), Coimbatore, India, 17–18 March 2017; pp. 1–4.

12. Dhami, A.; Parekh, N.N.; Vasavada, Y. Digital Beamforming for Antenna Arrays. In Proceedings of the 2019 IEEE Indian Conference on Antennas and Propogation (InCAP), Ahmedabad, India, 19–22 December 2019; pp. 1–5.
13. Jumaah, A.; Qasim, A. Hybrid Beamforming for Massive MIMO In 5G Wireless Networks. In Proceedings of the 4th Al-Noor International Conference for Science and Technology, Istanbul, Turkey, 13–18 August 2022.
14. Salunke, D.B.; Kawitkar, R.S. Analysis of LMS, NLMS and MUSIC Algorithms for Adaptive Array Antenna System. *Int. J. Eng. Adv. Technol.* **2013**, *2*, 130–133.
15. Senthilkumar, K.S.; Pirapaharan, K.; Hoole, P.R.P.; Hoole, R.R.H. Single Perceptron Model for Smart Beam Forming in Array Antennas. *Int. J. Electr. Comput. Eng. IJECE* **2016**, *6*, 2300. https://doi.org/10.11591/ijece.v6i5.10719.
16. Griffiths, L.J. A Simple Adaptive Algorithm for Real-Time Processing in Antenna Arrays. *Proc. IEEE* **1969**, *57*, 1696–1704. https://doi.org/10.1109/PROC.1969.7385.
17. Abdulkareem, A.; Farhan, M.J. A Novel MIMO Patch Antenna for 5G Applications. *IOP Conf. Ser. Mater. Sci. Eng.* **2020**, *870*, 012040. https://doi.org/10.1088/1757-899X/870/1/012040.
18. Khan, A.; Geng, S.; Zhao, X.; Shah, Z.; Jan, M.U.; Abdelbaky, M.A. Design of MIMO Antenna with an Enhanced Isolation Technique. *Electronics* **2020**, *9*, 1217. https://doi.org/10.3390/electronics9081217.
19. Kanagasabai, M.; Shanmuganathan, S.; Alsath, M.G.N.; Palaniswamy, S.K. A Novel Low-Profile 5G MIMO Antenna for Vehicular Communication. *Int. J. Antennas Propag.* **2022**, *2022*, 9431221. https://doi.org/10.1155/2022/9431221.
20. Sharma, S.; Arora, M. A Millimeter Wave Elliptical Slot Circular Patch MIMO Antenna for Future 5G Mobile Communication Networks. *Prog. Electromagn. Res. M* **2022**, *110*, 235–247.
21. Bakale, R.; Nandgaonkar, A.; Deosarkar, S. 4x4 Circularly Polarized Hexagonal Patch Antenna for Massive MIMO Base Station with Improved Isolation. In Proceedings of the 3rd International Conference on Communication and Information Processing(ICCIP), Tokyo, Japan, 24–26 November **2021.**
22. Zhang, X.-F.; Fan, J.; Chen, J.-X. High Gain and High-Efficiency Millimeter-Wave Antenna Based on Spoof Surface Plasmon Polaritons. *IEEE Trans. Antennas Propag.* **2019**, *67*, 687–691. https://doi.org/10.1109/TAP.2018.2879847.
23. Singh, H.; Mittal, N.; Gupta, A.; Kumar, Y.; Woźniak, M.; Waheed, A. Metamaterial Integrated Folded Dipole Antenna with Low SAR for 4G, 5G and NB-IoT Applications. *Electronics* **2021**, *10*, 2612. https://doi.org/10.3390/electronics10212612.
24. Cui, C.; Ren, Y.; Tao, P.; Cao, B. Microstrip Antenna with High Gain and Strong Directivity Loaded with Cascaded Hexagonal Ring-Shaped Metamaterial. *Materials* **2021**, *14*, 7289. https://doi.org/10.3390/ma14237289.
25. Sehrai, D.A.; Asif, M.; Khan, J.; Abdullah, M.; Shah, W.A.; Alotaibi, S.; Ullah, N. A High-Gain and Wideband MIMO Antenna for 5G Mm-Wave-Based IoT Communication Networks. *Appl. Sci.* **2022**, *12*, 9530. https://doi.org/10.3390/app12199530.
26. Balanis, C.A. *Antenna Theory Analysis and Design*; Chapter 2; John Wiley & Sons, INC: Hoboken, NJ, USA, 2005; p. 27.